Chapter 4
Conduction Velocity in Cardiac Tissue as Function of Ion Channel Conductance and Distribution

Kristian Gregorius Hustad[1], Ena Ivanovic[2], Adrian Llop Recha[3], Abinaya Abbi Sakthivel[3]

1 – Simula Research Laboratory, Norway
2 – Dept. of Physiology, University of Bern, Switzerland
3 – Dept. of Informatics, University of Oslo, Norway

Abstract Ion channels on the membrane of cardiomyocytes regulate the propagation of action potentials from cell to cell and hence are essential for the proper function of the heart. Through computer simulations with the classical monodomain model for cardiac tissue and the more recent extracellular-membrane-intracellular (EMI) model where individual cells are explicitly represented, we investigated how conduction velocity (CV) in cardiac tissue depends on the strength of various ion currents as well as on the spatial distribution of the ion channels. Our simulations show a sharp decrease in CV when reducing the strength of the sodium (Na^+) currents, whereas independent reductions in the potassium (K1 and Kr) and L-type calcium currents have negligible effect on the CV. Furthermore, we find that an increase in number density of Na^+ channels towards the cell ends increases the CV, whereas a higher number density of K1 channels slightly reduces the CV. These findings contribute to the understanding of ion channels (e.g. Na^+ and K^+ channels) in the propagation velocity of action potentials in the heart.

4.1 Introduction

A healthy heart rhythm is essential for the proper functioning of the cardiac pump, and requires the coordinated propagation of electrical impulses through the myocardium. The cardiac action potential is a change in the membrane potential governed by the ionic current flowing through ion channels, which are distributed along the cell membrane. Current flowing into the cell through activated sodium (Na^+) channels is responsible for the rapid upstroke of the action potential [1]. This is followed by

K. J. McCabe (ed.), *Computational Physiology*, Simula SpringerBriefs on Computing 12, https://doi.org/10.1007/978-3-031-05164-7_4

a current inflow through L-type calcium (CaL) channels and an outflow through different types of potassium channels (e.g. Kr and K1) leading to repolarisation, thus bringing the cell membrane to resting membrane potential [1]. More precisely, I_{Kr} is the rapid component of the delayed rectifier, and I_{K1}, the inward rectifying potassium current, which stabilises the resting membrane potential [1]. L-type calcium channels, on the other hand, are also responsible for the excitation-contraction coupling of the cardiac muscle [1].

Disorders of electrical conduction, such as slow conduction and conduction block, can lead to life-threatening arrhythmias, which occur frequently in the diseased heart. In this study, we investigated how both the strength of several transmembrane ionic currents and the spatial distribution of ion channels along the cell membrane influence conduction velocity (CV) in cardiac tissue. Our aim is to compare the effect on CV with the use of two computational models: the monodomain model and the extracellular-membrane-intracellular (EMI) model.

The monodomain model is a classical approximation of the electrical propagation in myocardial tissue based on a homogenised mathematical model of the cell. The intra- and extracellular domains overlap and are considered continuous. As a consequence, the monodomain model offers a good insight of large scale effects, but it is limited when sizes are reduced to a single cell. Alternatively, the EMI model represents the extracellular, the membrane, and the intracellular spaces at the expense of computational power. Therefore, one of the main advantages is the possibility to introduce changes in local cell properties (e.g. changes in ion channel density distribution on the cell membrane) that might contribute significantly to action potential propagation [2], [3].

4.2 Models and methods

4.2.1 The monodomain model

The monodomain model is a simplification of the bidomain model [4]. In the bidomain model, heart tissue is classified into two groups or domains: extracellular and intracellular, defined by their respective electric potentials, u_e and u_i, and conductivities $\boldsymbol{G_e}$ and $\boldsymbol{G_i}$.

Each point in the heart is considered to be in both domains. Therefore, both spaces overlap.

The physical description can be addressed using a generalisation of Ohm's Law. The current densities at each domain will be: $\boldsymbol{J_i} = -\boldsymbol{G_i}\nabla u_i$, and $\boldsymbol{J_e} = -\boldsymbol{G_e}\nabla u_e$. Assuming that there are no other sources than the membrane, the conservation of charge applies, and thus: $\nabla(\boldsymbol{J_i} + \boldsymbol{J_e}) = 0$.

The current flowing from one domain to the other through the cell membrane is called transmembrane current, I_m. Because the charge is conserved, then $\nabla \boldsymbol{J_e} = -\nabla \boldsymbol{J_i} = I_m$. Transmembrane current (Eq. 4.1) depends on the voltage drop between both domains, $v = u_i - u_e$, the membrane capacitance C_m, the ionic current, I_{ion}, and

surface area-to-volume ratio of cardiac cell, β_m.

$$I_m = \beta_m \left(C_m \frac{\partial v}{\partial t} + I_{\text{ion}}(v) \right) \tag{4.1}$$

It can be shown that the set of equations governing the bidomain model are the ones expressed in Eq.4.2 and Eq.4.3.

$$\nabla \boldsymbol{G_i} (\nabla v + \nabla u_e) = \beta_m \left(C_m \frac{\partial v}{\partial t} + I_{\text{ion}}(v) \right) \tag{4.2}$$

$$\nabla G_i \nabla v + \nabla (G_i + G_e) \nabla u_e = 0 \tag{4.3}$$

Solving the bidomain equation is a computationally heavy process. Therefore, the monodomain model is often used instead. In the monodomain model, the anisotropy between extra- and intracellular spaces is assumed to be the same, i.e., their respective conductances are proportional $\boldsymbol{G_i} = \lambda \boldsymbol{G_e}$.

If we define an effective conductivity, $\boldsymbol{G_{\text{eff}}} = \frac{\lambda}{1+\lambda} \boldsymbol{G_i}$, then the bidomain equation can be simplified and rearranged as shown in Eq.4.4.

$$\frac{\partial v}{\partial t} = \frac{1}{C_m \beta_m} \nabla \boldsymbol{G_{\text{eff}}} \nabla v - \frac{1}{C_m} I_{\text{ion}} \tag{4.4}$$

4.2.2 The EMI model

In the EMI model [5], the extracellular (E), cell membrane (M) and intracellular (I) domains, are represented explicitly as depicted in Figure 4.1. The intracellular spaces of both cells, Ω_i^1 and Ω_i^2, are separated from the extracellular domain, Ω_e, by the cell membrane boundaries, Γ_1 and Γ_2. Additionally, $\Gamma_{1,2}$ is the boundary separating the intracellular domains of two connected cells. Note that the EMI model is always solved in a three-dimensional space, as the extracellular space should be a single, connected domain.

The equation system describing the potentials in the EMI model is summarised in the following set of equations:

$$\begin{aligned}
\nabla \cdot \sigma_e \nabla u_e &= 0 && \text{in } \Omega_e, \\
\nabla \cdot \sigma_i \nabla u_i^k &= 0 && \text{in } \Omega_i^k, \\
u_e &= 0 && \text{at } \partial\Omega_e^D, \\
\boldsymbol{n_e} \cdot \sigma_e \nabla u_e &= 0 && \text{at } \partial\Omega_e^N, \\
u_i^k - u_e &= v^k && \text{at } \Gamma_k, \\
s_t^k &= F^k && \text{at } \Gamma_k,
\end{aligned}
\qquad
\begin{aligned}
\boldsymbol{n_e} \cdot \sigma_e \nabla u_e &= -\boldsymbol{n_i^k} \cdot \sigma_i \nabla u_i^k \equiv I_m^k && \text{at } \Gamma_k, \\
v^k &= \frac{1}{C_m} (I_m^k - I_{\text{ion}}^k) && \text{at } \Gamma_k, \\
\boldsymbol{n_i^2} \cdot \sigma_i \nabla u_i^2 &= -\boldsymbol{n_i^1} \cdot \sigma_i \nabla u_i^1 \equiv I_{1,2} && \text{at } \Gamma_{1,2}, \\
u_i^1 - u_i^2 &= w && \text{at } \Gamma_{1,2}, \\
w &= \frac{1}{C_{1,2}} (I_{1,2} - I_{\text{g}}^k) && \text{at } \Gamma_{1,2},
\end{aligned}$$

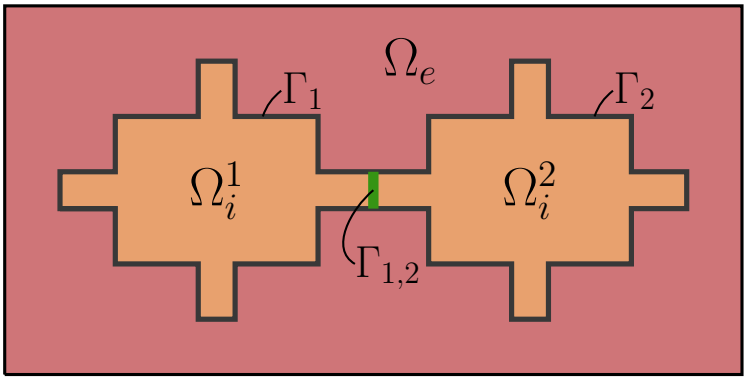

Fig. 4.1: Two-dimensional schematic of the different domains for two connected cells in the EMI model. Adapted from [5] with permissions dictated by the Creative Commons CC BY license (https://creativecommons.org/licenses/by/4.0/).

As in the case of the monodomain model, potentials of intracellular, extracellular and transmembrane domains are denoted by u_i, u_e and v, respectively. In addition to the ion current, I_{ion}, and the transmembrane current, I_m, defined at the cell membrane, Γ_k, a gap junction current, I_{g}, and a transmembrane current, $I_{1,2}$, are defined at the interface between two cells, $\Gamma_{1,2}$, in order to model the gap junction dynamics.

The gap junction between neighbouring cells, $\Gamma_{1,2}$, is modeled as a passive membrane with a constant resistance, R_g. Its electric dynamics are described using the currents I_g and $I_{1,2}$, and the potential drop at the junction, w.

Furthermore, C_m and $C_{1,2}$ are the transmembrane and the gap junction capacitances. σ_i and σ_e are the conductivities of both intracellular and extracellular domain, whereas $\boldsymbol{n_i}$ and $\boldsymbol{n_e}$ are the outward pointing normal vectors of the inner and outer cell domains, respectively.

The boundary of the extracellular domain, $\partial\Omega_e$, is further divided into two parts: one corresponding to the Dirichlet boundary conditions, $\partial\Omega_e^D$, and other one corresponding to the Neumann boundary conditions, $\partial\Omega_e^N$. Additionally, the index k can take the values 1 or 2 depending on which cell is described. Two cells were used to introduce the EMI model, however the model can easily be scaled up to consider more cells in the system.

Finally, s represents a collection of additional state variables introduced in the membrane model, whereas $F(v,s)$ represents the ordinary differential equations describing the dynamics of the additional state variables.

Since there is no analytical solution to the EMI model, a numerical solution is required (see [5, 3] for a discussion of numerical methods for the EMI model).

4.3 Results

We use code based on [6] to solve the monodomain and EMI models using finite difference method discretisation, and study the influence on CV. The simulations are run over a domain size of $2000\,\mu m \times 40\,\mu m$ for the monodomain model and $1956\,\mu m \times 40\,\mu m \times 30\,\mu m$ for the EMI model, both with a spatial resolution of $\Delta x = \Delta y = \Delta z = 2\,\mu m$. For the EMI model the cells are arranged in a line such that all cells are connected in the x direction, similar to Figure 4.1. Each cell is comprised of five disjoint subdomains, as depicted in Figure 4.3, and their extents are listed in Table 4.2. Regarding the time domain, the system evolves during 5 ms in steps of 0.01 ms.

The base model representing the cell membrane is described in [7]. Furthermore, the values of the most relevant parameters used in both monodomain and EMI model simulations are compiled in Table 4.1 and Table 4.2, respectively.

Parameter	Value
G_i (x direction)	$2.9\,mS\,cm^{-1}$
G_i (y direction)	$1.0\,mS\,cm^{-1}$
λ	2/3
C_m	$1.0\,\mu F\,cm^{-2}$
β_m	$2000\,cm^{-1}$

Table 4.1: Relevant parameter values used in the monodomain simulations.

Parameter	Value	Domain	Extent
C_m	$1.0\,\mu F\,cm^{-2}$	Ω_O	$100\,\mu m \times 20\,\mu m \times 20\,\mu m$
$C_{1,2}$	$1.0\,\mu F\,cm^{-2}$	Ω_N	$16\,\mu m \times 4\,\mu m \times 16\,\mu m$
σ_e	$20.0\,mS\,cm^{-1}$	Ω_S	$16\,\mu m \times 4\,\mu m \times 16\,\mu m$
σ_i	$4.0\,mS\,cm^{-1}$	Ω_W	$4\,\mu m \times 16\,\mu m \times 16\,\mu m$
R_g	$0.0045\,k\Omega\,cm^2$	Ω_E	$4\,\mu m \times 16\,\mu m \times 16\,\mu m$

Table 4.2: Relevant parameter values used in the EMI simulations.

Our study aims to investigate the CV dependence with ion channel properties from two different perspectives: when ion channel conductances change, and when ion channel distributions along the cell membrane is modified.

First, for exploring the relation between CV and ion channel conductance, we focused particularly on the Na^+, K1, Kr and CaL channels. The nominal values for the Na, K1 and Kr channel conductances are 12.6, 0.37 and $0.025\,mS\,\mu F^{-1}$, respectively, while the nominal value for CaL channel conductance is $0.12\,nL\,\mu F^{-1}\,ms^{-1}$ as

specified in [7]. Every conductance was varied from 20% to 150% of their respective nominal value by sweeping an adjustment factor from 0.2 to 1.5 in steps of 0.1.

Figure 4.2 shows the resultant CV dependence with each channel conductance in both models, the monodomain model and the EMI model.

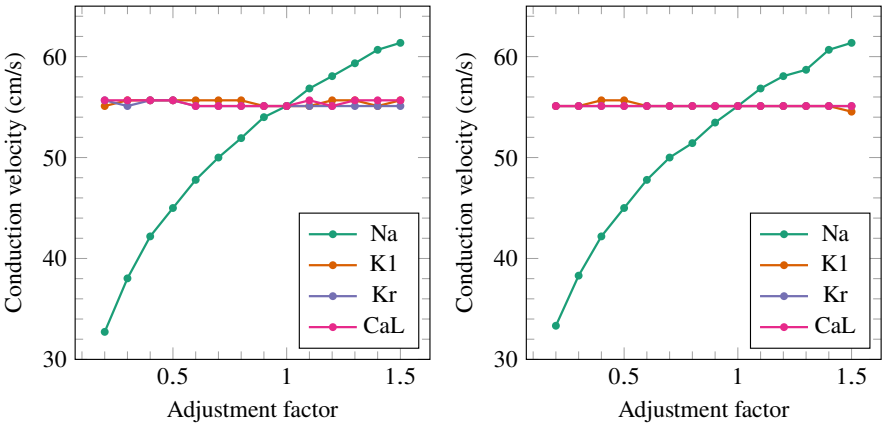

Fig. 4.2: CV dependence with channel conductance of Na, CaL, K1 and Kr channels simulated using (a) the monodomain and (b) EMI models.

In order to address the second part of our study, we change the uniform distribution of ion channels into a non-uniform distribution along the cell membranes. Changes in local properties of cells can only be implemented using the EMI model by allowing movement of ion channels towards the cell ends, i.e., the region that is closest to the $\Gamma_{1,2}$ domain (see Figure 4.1). To run the simulations, we considered two types of channels, Na^+ and K1, and we explored their four corner distribution states, i.e, when both Na^+ and K1 are uniformly distributed, when both type of channels are completely shifted towards the cell end (see Figure 4.3), and a combination of these two. The resulting CV for each case is compiled in Table 4.3.

	Uniform K1	Non-uniform K1
Uniform Na	55.1 cm/s	54.0 cm/s
Non-uniform Na	60.0 cm/s	58.7 cm/s

Table 4.3: CV (cm/s) with uniform and non-uniform channel distribution.

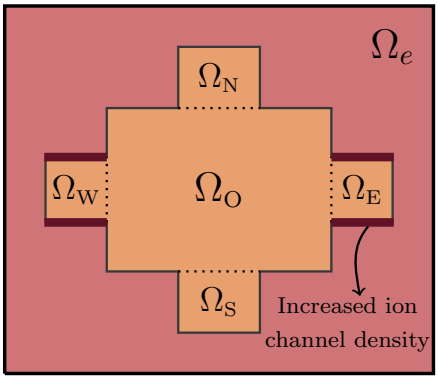

Fig. 4.3: In our simulations of a non-uniform distribution of ion channels, the ion channel density was increased in the brown areas near the cell ends (Ω_W and Ω_E) and decreased elsewhere (Ω_N, Ω_S and Ω_O).

4.4 Discussion

4.4.1 Influence of ion channel conductance on CV

Figure 4.2 shows that the CV increases monotonously as a function of the sodium channel conductance, g_{Na}, and this dependency is observed for both models.

To assess the compatibility between the monodomain and EMI model, the calculated CV points for Na^+ in Figure 4.2 are fitted into a function of the form $CV(g_{Na}) = a \cdot g_{Na}^p$, where a and p are constants, using a non-linear least-squares method. The curve adjustment is shown in Figure 4.4. For the constant p, we obtain $p = 0.294$ and $p = 0.3$ for the EMI model and the monodomain model, respectively. Thus, consistent results were obtained with both models.

Furthermore, Figure 4.2 shows that CV remains almost constant when sweeping K^+ and CaL channels conductances. Therefore, varying the strength of these ion channels did not lead to significant changes in CV.

4.4.2 Influence of ion channel distribution

From Table 4.3, when both K1 and Na^+ channels are uniformly distributed, the CV reaches 55.1 cm/s. However, when all Na^+ channels are placed at the cell ends (the coupling junction area between neighbouring cells) while keeping K1 channels uniformly distributed, then the CV experienced an increment of around

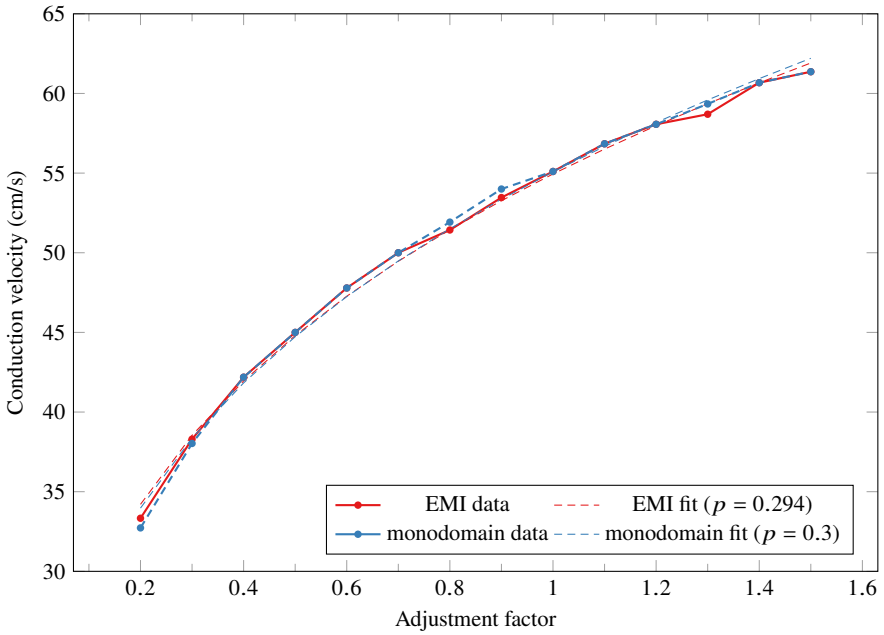

Fig. 4.4: Fitting the CV to the function $CV(g_{Na}) = a \cdot g_{Na}^{p}$.

9% with respect to the previous situation. Conversely, when K1 channels are moved towards the cell ends and Na^+ channels are kept uniformly distributed along the cell membrane, CV decreased around 2%.

These results suggest that Na^+ channel distribution contributes significantly to the overall CV, whereas the effect of K1 distribution is relatively small. While Na^+ channels increased the CV as their accumulation to the cell end increased, the opposite effect was observed with a non-uniform distribution of K1 channels. Additionally, we deduce that both contributions are asymmetrical. The displacement of Na^+ channels causes a major impact on CV compared to the displacement of K1 channels. When both channels are non-uniformly distributed, the CV increases about 6.5% (see Table 4.3). This CV is the result of the displacement of Na^+ channels, which largely increases CV, mitigated by the displacement of K1 channels, which slightly decreases CV.

Immunohistochemical studies revealed that about 50% of the Na^+ channels are located in the membranes of the intercalated discs [8]. In the diseased heart with reduced gap junctional coupling, action potential propagation can be maintained through a mechanism known as ephaptic coupling. A prerequisite for ephaptic effects to occur is a high density of Na^+ channels at the intercalated disc, where the intermembrane distance between two adjacent cells is small (< 30 nm, [9]).

4.5 Conclusions

In this study, we investigated the influence of ion channels, their conductance and their physical distribution along the cell membrane, on CV. To that end, two different models were used: the monodomain model and the EMI model. While the former offers a good insight of large scale effects by reducing the cell model complexity, the latter allows the implementation of changes in local cell properties, at the expense of increased computational effort.

Regarding the CV dependence on ion channel conductance, the study focused particularly on Na^+, K^+ (K1 and Kr) and CaL channels. Both models showed that Na^+ channel conductance strongly influences CV, whereas the effect of the other ion channel conductances on CV is negligible. Moreover, the changes in CV as a result of modifying Na^+ and K1 channels distribution on the cell membranes, were explored with the use of the EMI model. The simulation results suggest that the influence of these channels to the CV is opposed and asymmetrical. The influence is considered opposed because the CV increases, when Na^+ channels are moved towards the cell ends, but decreases in the case of K1 channels being located at the cell ends. Furthermore, the effect on CV is asymmetrical because the movement of Na^+ channels along the cell membrane causes a substantial modification of the CV, of around 9%, compared to the transfer of K1 channels, which accounts for a variation of 2%.

Acknowledgements The illustrations in Figure 4.1 and Figure 4.3 were created by Karoline Horgmo Jæger and reused with permission. The authors are grateful to Jæger for proofreading the manuscript and for providing code solving the monodomain and EMI models, and to Aslak Tveito for discussions about our findings in this study.

References

1. Bertil Hille. *Ionic channels of excitable membranes*. Sinauer Associates, Sunderland, MA, U.S.A., 1992.
2. RH Clayton, O Bernus, EM Cherry, H Dierckx, FH Fenton, L Mirabella, AV Panfilov, FB Sachse, G Seemann, and H Zhang. Models of cardiac tissue electrophysiology: Progress, challenges and open questions. *Progress in Biophysics and Molecular Biology*, 104(1):22–48, 2011. Cardiac Physiome project: Mathematical and Modelling Foundations.
3. Karoline Horgmo Jæger, Kristian Gregorius Hustad, Xing Cai, and Aslak Tveito. Efficient numerical solution of the emi model representing the extracellular space (e), cell membrane (m) and intracellular space (i) of a collection of cardiac cells. *Frontiers in Physics*, 8:539, 2021.
4. L Tung. *A bidomain model for describing ischemic myocardial D-C potentials.* PhD thesis, M.I.T. Cambridge, Mass., 1978.
5. Aslak Tveito, Karoline Horgmo Jæger, Miroslav Kuchta, Kent-Andre Mardal, and Marie E Rognes. A cell-based framework for numerical modeling of electrical conduction in cardiac tissue. *Frontiers in Physics*, 5:48, 2017.
6. Karoline Horgmo Jæger, Andrew G Edwards, Andrew McCulloch, and Aslak Tveito. Properties of cardiac conduction in a cell-based computational model. *PLOS Computational Biology*, 15(5):1–35, 05 2019.
7. Karoline Horgmo Jæger, Verena Charwat, Bérénice Charrez, Henrik Finsberg, Mary M Maleckar, Samuel Wall, Kevin E Healy, and Aslak Tveito. Improved computational identification of drug response using optical measurements of human stem cell derived cardiomyocytes in microphysiological systems. *Frontiers in Pharmacology*, 10:1648, 2020.
8. SA Cohen. Immunocytochemical localization of rh1 sodium channel in adult rat heart atria and ventricle. presence in terminal intercalated disks. *Circulation*, 94:3083–3086, 1996.
9. Y Mori, GI Fishman, and CS Peskin. Ephaptic conduction in a cardiac strand model with 3d electrodiffusion. *Proc Natl Acad Sci U S A*, 105:6463–6468, 2008.